Article:
Taylor-Mew, J.D. orcid.org/0000-0002-0895-2968, Petticrew, J.D. orcid.org/0000-0003-3424-2457, Tan, C.H. et al. (1 more author) (2022) Simulation of Al0.85Ga0.15As0.56Sb0.44 avalanche photodiodes. Optics Express, 30 (11). pp. 17946-17952. ISSN 1094-4087

https://doi.org/10.1364/oe.458922

Research Article | Vol. 30, No. 11 / 23 May 2022 / Optics Express 17946
Optics EXPRESS

Simulation of $Al_{0.85}Ga_{0.15}As_{0.56}Sb_{0.44}$ avalanche photodiodes

J. D. Taylor-Mew, J. D. Petticrew, C. H. Tan, and J. S. Ng*

Department of Electrical and Electronic Engineering, The University of Sheffield, Mappin Street, Sheffield, S1 3JD, UK
*j.s.ng@sheffield.ac.uk

Abstract: $Al_{0.85}Ga_{0.15}As_{0.56}Sb_{0.44}$ is a promising avalanche material for near infrared avalanche photodiodes (APDs) because they exhibit very low excess noise factors. However electric field dependence of ionization coefficients in this material have not been reported. We report a Simple Monte Carlo model for $Al_{0.85}Ga_{0.15}As_{0.56}Sb_{0.44}$, which was validated using reported experimental results of capacitance-voltage, avalanche multiplication and excess noise factors from five APDs. The model was used to produce effective ionization coefficients and threshold energies between 400–1200 kV.cm^{-1} at room temperature, which are suitable for use with less complex APD simulation models.

1. Introduction

Avalanche photodiodes (APDs) are widely used in high-speed optical communication [1] and laser ranging applications [2], which require detection of weak optical signals. In these applications, the detection system's signal-to-noise ratio is often limited by the electronic noise. An APD provides internal gain, termed avalanche multiplication, M, amplifying the optical signals before the electronics. This reduces the significance of electronic noise and increases the system's signal-to-noise ratio, making APDs advantageous compared to photodiodes.

Avalanche multiplication of an APD is the end product of successive impact ionization events taking place in its avalanche region. Impact ionization events are stochastic so there are fluctuations around a mean value of M for a given APD's reverse bias, V. This gives rise to APD's excess noise factor, F, which generally increases with M. The exact $F(M)$ characteristics depend on the avalanche material, operating temperature, and the avalanche region width, w.

Near infrared APDs grown on InP substrates usually have InP [3] or $In_{0.52}Al_{0.48}As$ [4–6] as their avalanche material. In recent years, the material $Al_{0.85}Ga_{0.15}As_{0.56}Sb_{0.44}$ (hereafter referred to as AlGaAsSb) has shown much potential as an alternative avalanche material, following reports of very low $F(M)$ characteristics [7–9], compared to other common avalanche materials [3–6]. There are however no accurate impact ionization coefficients for electrons and holes, α and β, for this material in the literature. It is therefore problematic to accurately simulate $M(V)$ and $F(M)$ characteristics as well as avalanche breakdown voltage, V_{bd}, for AlGaAsSb APDs.

Extracting impact ionization coefficients from experimental results of $M(V)$ and $F(M)$ usually require experimental samples with uniform electric fields across the avalanche regions. The AlGaAsSb diodes in Refs. [7,8] unfortunately possess relatively graded doping profiles, producing non-uniform electric field profiles. Commonly used APD simulation models, such as local model [10], recurrence model [11], and Random Path Length (RPL) model [12], are unsuitable for non-uniform electric field profiles [13]. Obtaining electric field dependences of α and β for AlGaAsSb therefore requires a more complex method and APD simulation model.

#458922 https://doi.org/10.1364/OE.458922
Journal © 2022 Received 21 Mar 2022; revised 20 Apr 2022; accepted 28 Apr 2022; published 9 May 2022

Optics EXPRESS

In this work, we present a Simple Monte Carlo (SMC) simulation model for AlGaAsSb APDs, which was validated with extensive, published room temperature data of $M(V)$ and $F(M)$ [7,8]. Using the AlGaAsSb SMC model, electric field dependences of impact ionization coefficients and threshold energies were extracted. These could be used with simpler, more accessible simulation models, such as recurrence model and RPL model, provided the APD designs have well-defined doping profiles.

2. Model

The SMC model used in this work is largely based on Ref. [14] and has been shown to work with InP [15] a III-V material and Si [16] an indirect bandgap material like AlGaAsSb. This work does contain a notable difference, with alloy scattering included as an additional scattering mechanism for the carriers as in an $In_{0.52}Al_{0.48}As$ SMC model [13]. In the simulation, each carrier drifts across an avalanche region, under an electric field, for a random distance before undergoing one of four possible scattering mechanisms: intervalley phonon emission, intervalley phonon absorption, impact ionization or alloy scattering. Carriers are tracked until they exit the avalanche region. A simulation ends when all carriers have left the avalanche region. When simulating an APD at a given reverse bias, the electric field profile was calculated using a 1-D Poisson's field solver.

The rate of intervalley phonon emission (R_{em}) and absorption (R_{ab}) is given by

$$R_{em} = \frac{N(T)+1}{\lambda\ (2N(T)+1)}\sqrt{\frac{2\,(E_c-\hbar\omega)}{m^*}}, \tag{1}$$

and

$$R_{ab} = \frac{N(T)+1}{\lambda\,(2N(T)+1)}\sqrt{\frac{2(E_c+\hbar\omega)}{m^*}}, \tag{2}$$

respectively. $\hbar\omega$ is phonon energy, m^* is effective mass of the free carrier, E_c is the carrier's energy, λ is mean free path, T is temperature, and $N(T)$ is the temperature dependent phonon occupation factor. $N(T)$ is given by $N(T) = (\exp((\hbar)\omega/kT)-1)^{-1}$, where k is Boltzmann's constant. The rate of impact ionization (R_{ii}) is calculated using the Keldysh equation [17]

$$R_{ii} = C_{ii}\left(\frac{E_c - E_{th}}{E_{th}}\right)^{\gamma}, \tag{3}$$

where C_{ii} is the prefactor of impact ionization rate, E_{th} is the SMC model's threshold energy for impact ionization, and γ is the softness factor. Alloy scattering rate (R_{alloy}) [13,18] is given by

$$R_{alloy} = C_{alloy}\,(m^*)^{\frac{3}{2}}\sqrt{E_c}, \tag{4}$$

where C_{alloy} is an alloy constant. For each carrier type (electron or hole), there is a probability table for these four scattering mechanisms interaction rate at a given energy.

Value of $\hbar\omega$ was obtained by linear interpolation of values from the binary materials [19–21]. Value of E_{th} was similarly obtained. Value of the binary material's threshold energy was given by the weighted average [22] $E_{th} = (E_0 + 3E_x + 4E_L)/8$, where E_0, E_x, and E_L [19,23–26] are the energy bandgap for Γ, X and L valleys, respectively.

3. Validation

Values of C_{ii}, E_{th} and C_{alloy} were adjusted so that the SMC results agree with published $M(V)$ and $F(M)$ results. The relative permittivity for this material was from [27] and built-in voltage was extracted from experimental Capacitance-Voltage (C-V) data. The AlGaAsSb SMC model

Optics EXPRESS

Table 1. $Al_{0.85}Ga_{0.15}As_{0.56}Sb_{0.44}$ SMC model parameter set

	Electrons	Holes
Phonon energy, $\hbar\omega$ (meV)	44	
Threshold energy, E_{th} (eV)	2	
Mean free path, λ (Å)	50	33
Effective mass, m^*	0.6 m_0	0.65 m_0
Impact ionization rate prefactor, C_{ii} ($\times 10^{12}$ s^{-1})	60	
Softness factor, γ	2	
Alloy scattering constant ($\times 10^{68}$)	1	3
Relative permittivity, ε_r	11.41 [27]	
Built-in voltage (V)	1.24	

parameter set is summarized in Table 1. The SMC predicts saturation velocities of 7.6×10^4 and 6.6×10^4 m.s^{-1} for electrons and holes respectively, close to those of GaAs.

The experimental data used in the SMC model validation were from three *p-i-n* wafers (A, C, and E) and two *n-i-p* wafers (B and D) of various AlGaAsSb avalanche widths, w, reported in Refs. [7,8]. Nominal w values, V_{bd} values, and data types of the wafers are summarized in Table 2. The *p-i-n* wafers provided validation data for electron-initiated avalanche multiplication and excess noise factor, $M_e(V)$ and $F_e(M_e)$, respectively. Similarly the *n-i-p* wafers provided hole-initiated avalanche multiplication and excess noise factor, $M_h(V)$ and $F_h(M_h)$.

Table 2. AlGaAsSb APDs used to validate the SMC model

Wafer	Structure	w (nm)	V_{bd} (V)	Data
A [3]	*p-i-n*	80	11.0	$M_e(V)$; $F_e(M_e)$
B [3]	*n-i-p*	98	10.6	$M_h(V)$; $F_h(M_h)$
C [3]	*p-i-n*	160	15.9	$M_e(V)$; $F_e(M_e)$
D [3]	*n-i-p*	193	15.9	$M_h(V)$; $F_h(M_h)$
E [4]	*p-i-n*	608	37.2	$M_e(V)$; $F_e(M_e)$

The doping profiles for wafer A-D used were estimated from C-V data and Secondary Ion Mass Spectroscopy. For each of the five wafers, the C-V data used cover multiple devices with at

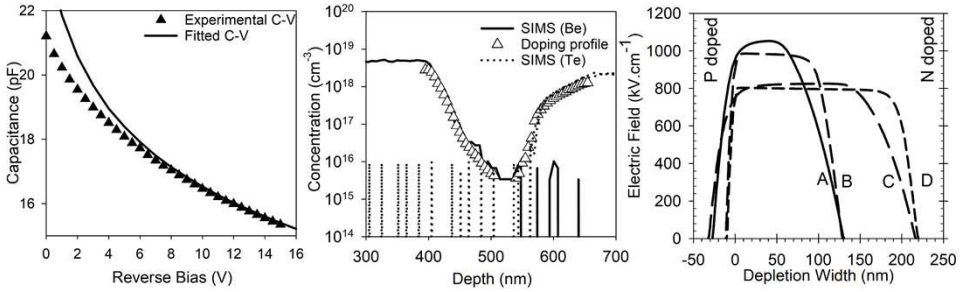

Fig. 1. (Left) Experimental C-V characteristics and fitting using 1-D Poisson's field solver for wafer C with device diameter of 109.3 µm. (Middle) Doping profiles used in C-V fitting and from SIMS results. (Right) Electric field profiles of wafer A-D at 98% of their breakdown voltages.

Optics EXPRESS

least three device diameters. In addition, C-V data analyses included slight reductions in device area to account for device fabrication tolerances.

The C-V data and fitting using the 1-D Poisson's field solver for wafer C (109.3 μm device diameter) are shown as examples in Fig. 1(left). The doping profile used for C-V fitting (and subsequently SMC simulations) was extracted from SIMS data, both of which are shown in Fig. 1(middle). This process was applied to all other wafers, with the exception of wafer E whose C-V data were fitted satisfactorily using a 3-region fitting. Examples of electric field profiles of wafers A-D (at 98% of their breakdown voltages) are shown in Fig. 1 (right).

Using our SMC model, avalanche multiplication and excess noise characteristics were simulated for wafers A, C and E (electron-initiated) as well as wafers B and D (hole-initiated). The simulated results are in agreement with the validation data (experimental results), as shown in Fig. 2.

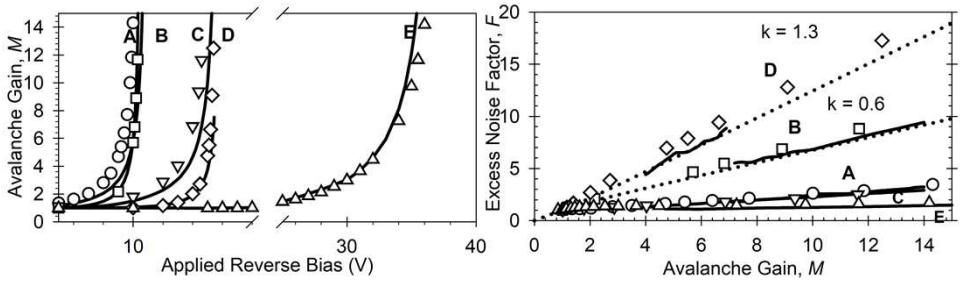

Fig. 2. (Left) $M(V)$ and (Right) $F(M)$ from the SMC model (symbols) are in agreement with the validation data from Refs. [3,4] (lines). Dotted lines indicate the McIntrye's local excess noise model [10], where k is ionization ratio.

4. Results

Using the AlGaAsSb SMC model, another series of simulations were carried out to extract impact ionization coefficients as functions of electric field (ξ) from 400 to 1200 kV.cm^{-1}. For this, each simulation tracked a single carrier (electron or hole) under a constant electric field of infinite length and recorded distances between each consecutive impact ionisation events (i.e. ionization path lengths). These statistics yielded probability density functions (PDFs) of the ionization path lengths for electrons and holes, $h_e(x)$ and $h_h(x)$ [28]. Effective ionization coefficient (α^* and β^*) and deadspace (d_e and d_h) for electrons and holes were obtained from fittings to these PDFs, using the hard deadspace assumption [11], where

$$h_e(x) = \begin{cases} 0, & x \le d_e \\ \alpha^* \exp[-\alpha^*(x - d_e], & x > d_e \end{cases} . \tag{5}$$

Example $h_e(x)$ and $h_h(x)$ as well as their fittings at $\xi = 800$ kV.cm^{-1} are shown in Fig. 3(left). For each electric field, values of α^* (or β^*) and d_e (or d_h) were extracted by fitting to the gradient of $h_e(x)$ at large x and the $h_e(x)$ region before the peak, respectively. The deadspaces were given by $d_{e(h)} = E_{the(h)}/q\xi$, where E_{the} and E_{thh} are threshold energy for electrons and holes, respectively.

The values for E_{the} and E_{thh} are 3.6 eV. The extracted α^* and β^* are plotted versus inverse electric field in Fig. 3(right). They can be parametrized using

$$\alpha^*(\xi) = 5.2 \times 10^6 \exp\left[-\left(\frac{1.8 \times 10^6}{\xi}\right)^{1.27}\right] \text{cm}^{-1} \tag{6}$$

Optics EXPRESS

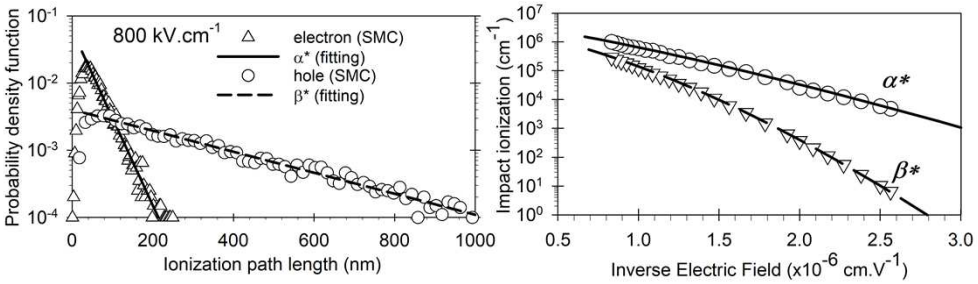

Fig. 3. (Left) Probability density function of ionization path length from SMC (symbols) and fittings (lines) at 800 kV.cm-1. (Right) α^* and β^* obtained from the SMC model (symbols) and the parameterized expressions (lines).

and

$$\beta^*(\xi) \;=\; 3.2\times 10^6 \exp\left[-\left(\frac{2.1\times 10^6}{\xi}\right)^{1.53}\right] \mathrm{cm}^{-1}, \tag{7}$$

which are also included in Fig. 3(right).

To confirm the validity of Eqn. (1) and (2), avalanche multiplication and excess noise factors of a series of AlGaAsSb ideal *p-i-n* diodes were simulated using both the AlGaAsSb SMC model and an RPL model. Inputs to the latter are Eqn. (6) and (7) as well as our E_{the} and E_{thh} values. The ideal *p-i-n* diodes, labelled as D1, D2, D3, D4, D5, and D6, have w of 100, 200, 500, 800, 1000, and 1500 nm, respectively. Results from SMC and RPL simulations are in good agreement, as shown in Fig. 4, confirming the validity of our expressions for $\alpha^*(\xi)$, $\beta^*(\xi)$, E_{the}, and E_{thh}.

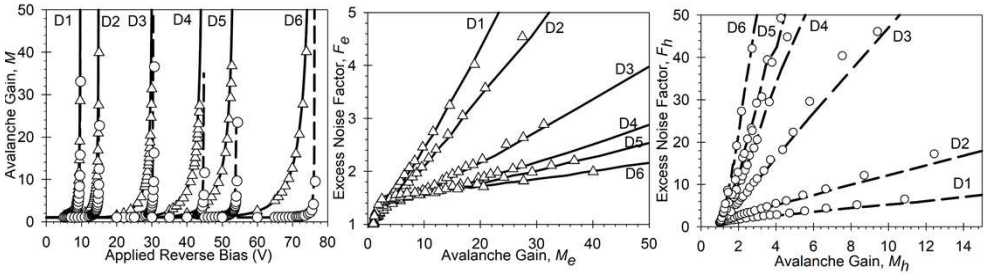

Fig. 4. Comparisons of (left) $M(V)$, (middle) $F_e(M_e)$, and (right) $F_e(M_e)$ simulated using SMC (triangle for electron- and circles for hole-initiated conditions) and RPL (solid lines for electron- and dashed lines for hole-initiated conditions). D1, D2, D3, D4, D5, and D6 have w of 100, 200 500, 800, 1000, and 1500 nm, respectively.

Simulation results for D5 ($w = 1000$ nm) indicate V_{bd} of 54 V, which is consistent with the 1000 nm AlGaAsSb APD reported in [9]. It is however lower than the 58 V reported in [29] for a $w = 910$ nm AlGaAsSb APD, possibly due to experimental uncertainties in the APD structure.

5. Conclusion

We have presented an SMC model for $Al_{0.85}Ga_{0.15}As_{0.56}Sb_{0.44}$ APDs at room temperature. The model was validated using comprehensive experimental results of capacitance-voltage, avalanche multiplication, and excess noise factor from earlier reports on $Al_{0.85}Ga_{0.15}As_{0.56}Sb_{0.44}$ APDs. Using this validated model, we have extracted room temperature electric field dependences of effective impact ionization coefficients and threshold energies for $Al_{0.85}Ga_{0.15}As_{0.56}Sb_{0.44}$ at

Optics EXPRESS

electric field range of 400–1200 kV.cm^{-1}. These parameters can be used with RPL model and recurrence equations for $Al_{0.85}Ga_{0.15}As_{0.56}Sb_{0.44}$ APD simulations of avalanche multiplication and excess noise factors.

Funding. UK Engineering and Physical Sciences Research Council (EP/N509735/1).

Disclosures. The authors declare no conflicts of interest.

Data availability. Data underlying the results presented in this paper are available in Ref. [30].

References

1. V. Shulyak, M. M. Hayat, and J. S. Ng, "Sensitivity Calculations of High-Speed Optical Receivers Based on Electron-APDs," J Lightwave Technol **38**(4), 989–995 (2020).
2. A. M. Pawlikowska, A. Halimi, R. A. Lamb, and G. S. Buller, "Single-photon three-dimensional imaging at up to 10 kilometers range," Opt Express **25**(10), 11919 (2017).
3. L. J. J. Tan, J. S. Ng, C. H. Tan, and J. P. R. David, "Avalanche Noise Characteristics in Submicron InP Diodes," IEEE J. Quantum Electron. **44**(4), 378–382 (2008).
4. Y. L. Goh, A. R. J. Marshall, D. J. Massey, J. S. Ng, C. H. Tan, M. Hopkinson, J. P. R. David, S.K. Jones, and C. C. Button, "Excess Avalanche Noise in $In_{0.52}Al_{0.48}As$," IEEE J. Quantum Electron. **43**(6), 503–507 (2007).
5. W. Wang, J. Yao, J. Wang, Z. Deng, Z. Xie, J. Huang, H. Lu, and B. Chen, "Characteristics of thin InAlAs digital alloy avalanche photodiodes," Opt. Lett. **46**(16), 3841 (2021).
6. J. Zheng, Y. Yuan, Y. Tan, Y. Peng, A. K. Rockwell, S. R. Bank, A. W. Ghosh, and J. C. Campbell, "Digital Alloy InAlAs Avalanche Photodiodes," J. Lightwave Technol. **36**(17), 3580–3585 (2018).
7. L. L. G. Pinel, S. J. Dimler, X. Zhou, S. Abdullah, S. Zhang, C. H. Tan, and J.S. Ng., "Effects of carrier injection profile on low noise thin Al0.85Ga0.15As0.56Sb0.44 avalanche photodiodes," Opt Express **26**(3), 3568 (2018).
8. J. Taylor-Mew, V. Shulyak, B. White, C. H. Tan, and J. S. Ng, "Low Excess Noise of $Al_{0.85}Ga_{0.15}As_{0.56}Sb_{0.44}$ Avalanche Photodiode From Pure Electron Injection," IEEE Photonics Technol. Lett. **33**(20), 1155–1158 (2021).
9. S. Lee, S. H. Kodati, B. Guo, A. H. Jones, M. Schwartz, M. Winslow, C.H. Grein, T. J. Ronningen, J. C. Campbell, and S. Krishna, "Low noise $Al_{0.85}Ga_{0.15}As_{0.56}Sb_{0.44}$ avalanche photodiodes on InP substrates," Appl. Phys. Lett. **118**(8), 081106 (2021).
10. R. J. McIntyre, "Multiplication noise in uniform avalanche diodes," IEEE Trans. Electron. Devices **ED-13**(1), 164–168 (1966).
11. M. M. Hayat, B. E. A. Saleh, and M. C. Teich, "Effect of dead space on gain and noise of double-carrier-multiplication avalanche photodiodes," IEEE Trans. Electron. Devices **39**(3), 546–552 (1992).
12. D. S. Ong, K. F. Li, G. J. Rees, J. P. R. David, and P. N. Robson, "A simple model to determine multiplication and noise in avalanche photodiodes," J appl phys **83**(6), 3426–3428 (1998).
13. S. C. Liew Tat Mun, C. H. Tan, Y. L. Goh, A. R. J. Marshall, and J. P. R. David, "Modeling of avalanche multiplication and excess noise factor in In0.52Al0.48As avalanche photodiodes using a simple Monte Carlo model," J. Appl. Phys. **104**, 013114 (2008).
14. J. D. Petticrew, S. J. Dimler, and J. S. Ng, "Simple Monte Carlo Simulator for Modelling Linear Mode and Geiger Mode Avalanche Photodiodes in C++," J. Open. Res. Softw **6**(1), 17 (2018).
15. J. D. Petticrew, S. J. Dimler, C. H. Tan, and J. S. Ng, "Modeling Temperature-Dependent Avalanche Characteristics of InP," J. Lightwave Technol. **38**(4), 961–965 (2020).
16. J. D. Petticrew, S. J. Dimler, X. Zhou, A. P. Morrison, C. H. Tan, and J. S. Ng, "Avalanche Breakdown Timing Statistics for Silicon Single Photon Avalanche Diodes," IEEE J. Sel. Top. Quantum Electron. **24**(2), 1 (2018).
17. L. V. Keldysh, "Kinetic theory of impact ionization in semiconductors," Sov. Phys. JETP **37**(10), 509–518 (1960).
18. M. A. Littlejohn, J. R. Hauser, T. H. Glisson, D. K. Ferry, and J. W. Harrison, "Alloy scattering and high field transport in ternary and quaternary III–V semiconductors," Solid State Electron **21**(1), 107–114 (1978).
19. S. Adachi, "Lattice Dynamic Properties" and "Energy-band Structure: Energy-band Gaps" in Properties of semiconductor alloys: group-IV, III-V and II-VI semiconductors. Chichester, U.K: Wiley, (2009).
20. Z. C. Feng, S. Perkowitz, R. Rousina, and J. B. Webb, "Raman and infrared spectroscopy of $In_{1-x}Ga_xSb$ films grown on GaAs by metal-organic magnetron sputtering," Can. J. Phys. **69**(3-4), 386–389 (1991).
21. R. Manor, O. Brafman, and R. F. Kopf, "Charge transfer between In and Ga in InGaAs-based alloys," Phys. Rev. B **56**(7), 3567–3570 (1997).
22. J. Allam, ""Universal" Dependence of Avalanche Breakdown on Bandstructure: Choosing Materials for High-Power Devices," Jpn. J. Appl. Phys. **36**(Part 1, No. 3B), 1529–1542 (1997).
23. J. L. Aubel, U. K. Reddy, S. Sundaram, W. T. Beard, and J. Comas, "Interband transitions in molecular-beam-epitaxial $Al_xGa_{1-x}As$/GaAs," J. Appl. Phys **58**(1), 495–498 (1985).
24. D. E. Aspnes, S. M. Kelso, R. A. Logan, and R. Bhat, "Optical properties of $Al_xGa_{1-x}As$," J. Appl. Phys **60**(2), 754–767 (1986).
25. A. K. Saxena, "Non-Γ Deep Levels and the Conduction Band Structure of $Ga_{1-x}Al_xAs$ Alloys," phys. stat. sol. (b) **105**(2), 777–787 (1981).
26. C. Alibert, A. Joullié, A. M. Joullié, and C. Ance, "Modulation-spectroscopy study of the $Ga_{1-x}Al_xSb$ band structure," Phys. Rev. B **27**(8), 4946–4954 (1983).

Optics EXPRESS

27. X. Zhou, S. Zhang, J. P. R. David, J. S. Ng, and C. H. Tan, "Avalanche Breakdown Characteristics of $Al_{1-x}Ga_xAs_{0.56}Sb_{0.44}$ Quaternary Alloys," IEEE Photonics Technol. Lett. **28**(22), 2495–2498 (2016).
28. S. A. Plimmer, J. P. R. David, and D. S. Ong, "The merits and limitations of local impact ionization theory," IEEE Trans. Electron Devices **47**(5), 1080–1088 (2000).
29. S. Lee, B. Guo, S. H. Kodati, H. Jung, M. Schwartz, A. H. Jones, M. Winslow, C. H. Grein, T. J. Ronningen, J. C. Campbell, and S. Krishna, "Random alloy thick AlGaAsSb avalanche photodiodes on InP substrates," Appl. Phys. Lett. **120**(7), 071101 (2022).
30. ORDA digital repository, doi: 10.15131/shef.data.19299665